Desalination and Water Treatment
www.deswater.com

doi: 10.5004/dwt.2022.28974

276 (2022) 40–49
November

An experimental investigation of the novel standalone vapour-based multistage solar still with stacked stages

Mfanafuthi Mthandeni Mkhize*, Velaphi Msomi

Cape Peninsula University of Technology, Faculty of Engineering and the Built Environment, Mechanical Engineering Department, P.O. Box 1906, Bellville, 7535, South Africa, emails: sggamkhize@gmail.com (M.M. Mkhize), msomiv@gmail.com (V. Msomi)

Received 11 May 2022; Accepted 4 October 2022

ABSTRACT

This work presents 2 days of experimental test results of the novel standalone vapour-based multistage solar still with stacked stages (MSS-SS) for the spring season. MSS-SS desalinate saline water (SW) through a series of stacked stages driven by solar energy. The study seeks to contribute to the body of knowledge in the field of solar energy desalination. It also introduces an MSS-SS aimed at minimizing maintenance requirements, thus, allowing these devices a prolonged and uninterrupted operation. Further, it presents a novel configuration with waterless stages that make the condensing assembly lightweight and easy to handle. The work was a developmental study conducted through experimental observation, data collection and analysis to obtain results. It was found that the continuous mode of thermal energy input caused thermal damage conditions, marginal distillate yield enhancement of 7.27% for the average solar radiation increment of 52.03%, thermal energy storage was required due to the larger collector-to-basin area ratio and insufficient thermal energy storage capacity in the SW due to its limited quantity. A 5,090 and 5,460 mL daily cumulative distillate yield for the impulsive and continuous modes were recorded, respectively. The study's benefit will be enabling remote geographical areas to easily produce freshwater from SW.

Keywords: Renewable energy; Distillation; Multistage still; Solar still; Stand-alone still

1. Introduction

Solar stills generally use thermal energy, direct or indirect, from the sun to heat and vaporise salty water in the basin [1,2]. They are renewable energy devices producing distilled water through thermal or hybrid methods. There are various types of solar stills in existence, such as cone, CPC-TSS pyramid, pit, double-basin double-sloped basin type, portable single basin, demo, corrugated, wick, inclined solar panel basin, triangular solar still, etc. Solar stills are categorised as passive and active solar stills [3]. Passive solar stills are solely driven by direct heating by solar radiation from the sun. At the same time, active solar stills are either indirectly heated or through the combination of direct or indirect heating by the sun and the solar collector [2]. Solar stills, whether passive or active, depends on the availability of solar radiation as a primary source of energy [1–3]. The performance of a solar still is generally guided by various conditions, including meteorological conditions such as solar radiation intensity, wind velocity, salinity levels in SW, etc. Design conditions refer to the designing and construction of solar still to maximise solar radiation captured, and distillate produced while reducing thermal energy loss. Operating conditions relate to parameters such as SW level in the solar still, the orientation of the still, nature of thermal energy input into the solar still, feed water inlet temperature, thickness of the thermal insulation material etc. [4,5]. However, solar

* Corresponding author.

radiation as a primary energy source in a solar still varies based on the time of the day, time of year and the latitude of the local location [6]. Furthermore, solar radiation as a primary thermal energy source tends to experience fluctuating distillate output due to the intermittent nature of solar intensity [7]. Various researchers have reported the range of solar stills over time, but new developments in the literature indicate continuous improvements in understanding factors affecting solar still performance [8].

However, the current study's attention is narrowed down to MSS-SS. The MSS-SS found in the literature surveyed consists of a waterbed in the stages [9–13]. A waterbed is the SW in the stacked stages of the MSS-SS used as an evaporative surface to produce the vapour, and is categorised as a stagnant waterbed and flowing waterbed [3,13,14]. Further, the stage trays' tilt angle ranges from 8° to 25° and can be shaped into either V-shape or A-shape for distillate collection [3,13,15]. Thermal energy can be supplied indirectly or by a combination of direct and indirect via solar collectors into the entry stage (bottom-most stage) and the uppermost stage [9,16]. Moreover, thermal energy supply to the intermediate stages uses latent heat of condensation through a sequential mode. The bottom-most stage (stage 1) transfers its latent heat of condensation to stage 2, then from stage 2 to stage 3, from stage 3 to stage 4 etc. [10,11]. However, various factors often affect the flow of thermal energy from low to upper stages in the condensing tower. For instance, the Estahbanati et al. [17] reported that the low heat transfer efficiency is because of heat loss from the walls, vapour condensing on the walls and other parts/components where it cannot be collected, droplets dropping back into the pool of SW, removal of some thermal energy with freshwater and device's operation in unsteady mode resulting in the storage of some energy at the end of the experiment. Moreover, the ability of the stage tray to transfer heat is affected by the algae growth and scaling on the stage trays since the SW stays in constant contact with the stage trays. Therefore, stage trays occasionally require cleaning [16–18]. However, Schwarzer et al. [10] reported that the saltwater residue accumulation can be avoided by SW circulation on the stage trays. The current study can add that brine disposal during operation also removes some thermal energy.

Further, the MSS-SS system incorporates equipment such electrical-driven pumps, electric heaters, and control units to produce freshwater [3,9,11–17]. Abdessemed et al. [15], Singh et al. [19], Bait and Si-Ameur [20], Shatat and Mahkamov [13] reported MSS-SS systems operating at maximum SW temperatures of 62°C, 53.7°C, 80.96°C and 100°C, respectively, driven by the one or the other electrical equipment. However, Schwarzer et al. [12] reported a standalone MSS-SS with no need of additional equipment consisting of 5 to 7 stages. It operated at SW temperatures of 95°C–100°C; therefore, it can be categorised as high temperature active solar distillation system. Moreover, the system used distilled water as the heat transfer fluid (HTF) to prevent corrosion in the collector manifold. The design incorporated a heat recovery configuration that transferred the latent heat of condensation sequentially to successive stages [9,13]. The SW was supplied from the topmost stage with gravitational influence [9]. Due its larger thermal energy storage capacity constituted by a larger body of SW in the stages, the SW temperature was reported to be at 80°C after sunset and at 45°C by the following morning, which increased its productivity during the nighttime [18]. The experimental and simulated work was conducted in four different geographical locations: Germany, India, Spain, and Brazil. The simulated work was conducted in a laboratory using an electric heater on single stage set-up. The fieldwork consisted of four prototypes divided into two energy source types, the flat plate solar collector (FPSC) and the evacuated tube solar collector (ETSC). A distillate yield from potable water used as feed water was 32–60 L/d under solar intensity of 6–8 kWh/m^2 and collector areas of 5 and 2.2 m^2 for the FPSC and ETSC, respectively. However, there was a reduction of 20% in productivity when SW was used as feed water. Furthermore, the condensing tower required stage cleaning since the SW stayed in contact with the stage trays. The quality test for distillate produced found that 98% of incondensable, potentially harmful solids were removed.

It has been observed that the previously studied solar still systems require electrical energy to drive some of the components or devices to control water flow. This paper aims to report the performance of a standalone vapour-based MSS-SS system that does not use electrical components for its operation. The full details about the construction of the system and its operating principle can be found in the literature [21]. The 2 days considered in this work were selected based on the distinct solar conditions. These two different solar conditions are sufficient to analyse the performance of the system which leads to a concrete conclusion.

2. Experimental setup

The experimental work in the current study consists of three major units: passive single slope single basin solar still (BSS), vapour-based condensing tower and two series connected evacuated tube solar collectors (ETSCs). Fig. 1 shows a schematic diagram of the vapour-based MSS-SS with five stacked stages integrated with the passive (BSS). Vapour-based refers to the absence of SW on stage trays constituting a vapour-based MSS-SS that is a standalone solar still system [12]. SW flow through the condensing tower is represented by coloured arrows indicating heat accumulation in the SW. The SW was at room temperature from the external tank, and the initial SW preheating occurred in the BSS. The SW then proceeded to flow under gravitational influence from the BSS and through stages 5 to 1 in a zigzagged SW tube, where further preheating occurred due to the vapour entering the stages. The five stacked stages were supplied with the vapour directly by the evaporator, eliminating the sequential heat transfer between the stages. The vapour was supplied through five vapour make-up tubes mounted vertically onto the evaporator. On one end, they were connected to the evaporator; on the other, they were connected to their respective stages.

The distillate was collected separately from each stage through distillate collecting points. SW was supplied from a 20-litres external tank adjacent to the BSS supported by the stand. All the SW in the system was supplied through gravitational influence and was remotely controlled and

regulated by the float valves. Preheated SW was then stored in the secondary tank and was occasionally sucked into the evaporator due to diminishing SW because of evaporation in the evaporator. Stages 2–5 were also fitted with vapour transfer tubes; in case of pressure build-up in the stages, these tubes transferred the vapour sequentially to the proceeding stage. Furthermore, the larger orange and the red arrows represent hot SW circulated between the evaporator and the series connected ETSCs.

Fig. 2 shows the complete test rig with its thermal energy supplied from the two series connected evacuated solar tube collectors [3]. The SW circulation in the ETSCs was driven by the thermodynamic principle of pressure differential caused by temperature and pressure increase in the pipeline fitted with a non-return valve. SW circulated impulsively or continuously in an open loop depending on solar radiation intensity. SW heating in the open loop created a one-directional SW flow in the pipeline, effectively replacing the electrically driven pumps for SW circulation in the system, hence, a standalone system.

The body of the condensing tower was made from a 0.9 mm thick aluminum sheet metal, and all the tubes from copper materials with a 15 mm external diameter. A 25 mm thick polystyrene material was used to insulate the body of the condensing tower to minimise heat losses. The evaporator was insulated with a 50 mm thick glass wool thermal insulation. The stages of the condensing tower were made into V-shapes for distillate collection [15]. Since no water-bed was present in the stages, the vapour was cooled and condensed by the SW in the zig-zagged tube shown in Fig. 3. The system had a built-in SW pre-heating and heat recover using the vapour exchanging heat with the relatively

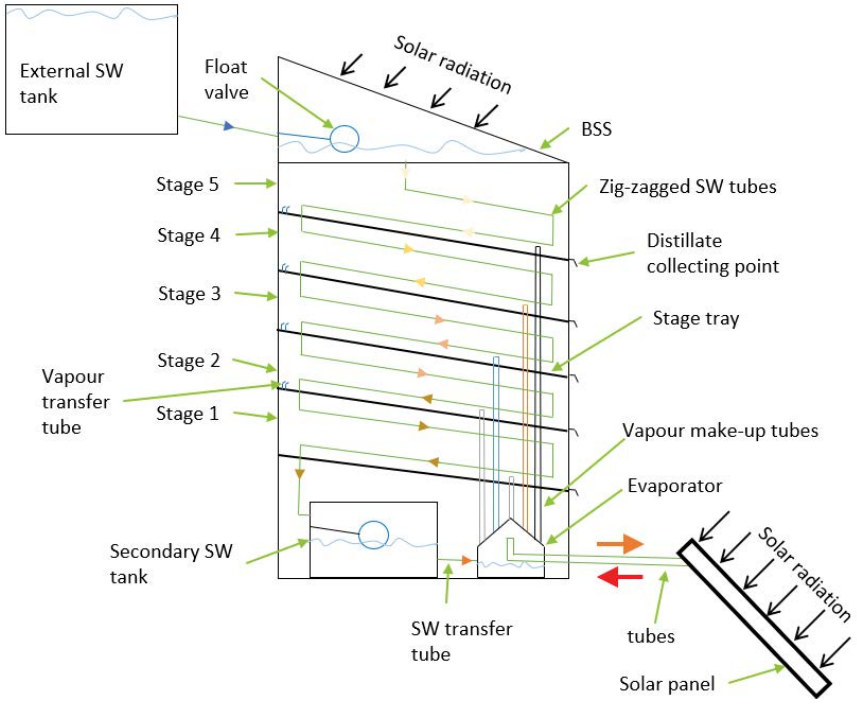

Fig. 1. Schematic diagram of the vapour-based MSS-SS.

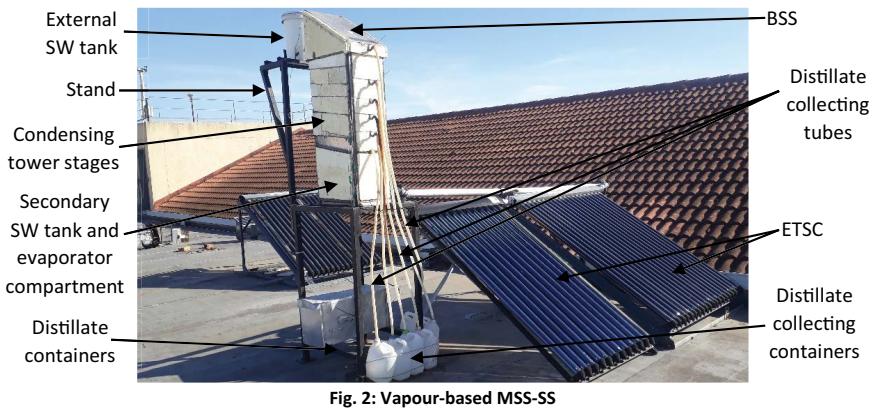

Fig. 2. Vapour-based MSS-SS.

cold SW in the zig-zagged tube. The system was built so that no cold SW at room temperature entered the evaporator. Therefore, all the SW entering the evaporator had been preheated to maintain and maximise the evaporation process. There was no distillate collecting troughs inside the stages as there was no waterbed [13,15]. In essence, no distillate loss by falling back into the pool of SW [17].

Furthermore, Fig. 3 shows the 3D internal components of the condensing tower of the MSS-SS produced by SOLIDWORKS. Firstly, it shows a transparent evaporator at the bottom of the stacked stages. It also shows the SW transfer tube connected to the secondary tank and the tube delivering heated SW from the ETSCs. The evaporator was then attached to five vapour make-up tubes shown in yellow colour. Secondly, it shows five V-shapes stage trays to collect the condensate from separate stages. Thirdly, it shows a zig-zagged tube in blue colour for delivering SW into the secondary tank, recover latent heat of condensation from vapour, preheat the SW as it flows down through each stage and providing the cooling surface for the vapour. Fourthly, it shows the secondary tank used to store preheated SW before transferring it into the evaporator for further heating and evaporation.

3. Experimental procedure

The vapour-based MSS-SS was experimentally tested under the climatic conditions of South Africa, Cape Town. Feed water for experimental tests was collected from Monwabisi beach in Khayelitsha. The MSS-SS was primed (removal of any air bubbles) with SW before the start of the operation. When the SW in the evaporator was evaporated, it diminished, or its quantity was reduced. That triggered the float valve in the secondary tank to open slightly, allowing SW in the zig-zagged tube to flow down into the secondary tank.

The SW from the BSS replaced the SW in the zig-zagged tube and the SW from the external tank replaced the SW in the BSS. Each time the secondary SW tank float valve opened, the above procedure would repeat, maintaining a fully primed system with no air bubbles. There were 12 K-type thermocouple probes used throughout the system to detect temperature variations. Amongst the 12 probes, one was installed on the stage 2 wall, another on the stage 2 tray to detect the variations on the condensing surfaces, another five installed on the outer surface of the zig-zagged tube in each stage, and two were in the BSS, one in the evaporator, one in the secondary SW tank and the last one in the external tank. A BTM-4208SD temperature data logger with 12 channels was used to collect temperature data from the system. A HP2000 wireless weather station was used to capture solar radiation intensity, wind velocity and ambient temperature, among others. Even though solar radiation ceased somewhere after sunset, the data was collected for 24 h/d. The SW quantities in the secondary tank and the evaporator were maintained at approximately 2.8 and 1.7 L, respectively. However, due to the SW depth and the circulation requirements, the SW at any time in the evaporator was approximately 0.5 kg. Six 5-L water containers (Fig. 2) were used to collect the distillate in the early morning of each day. The experimental test day lasted for 24 h, and started in the morning. Therefore, the distillate was only collected the following morning. A graduated cylinder with a maximum capacity of 1,000 mL (1 L) was used to measure the quantity of freshwater produced.

4. Results and discussions

4.1. Experimental test 1

Solar radiation, wind velocity and the ambient temperature for the location of Cape Town, South Africa location were collected. The data presented in this subsection is from the 26th of Sept. 2020 in the spring season. The prevailing solar irradiance on the day is shown in Fig. 4. The solar irradiance was recorded from just after 6 AM to after 6 PM, with heavy fluctuations indication an impulsive mode of thermal input [13]. It peaked at 1,037 W/m^2 with a daily average value of 253.7 W/m^2. The average was calculated

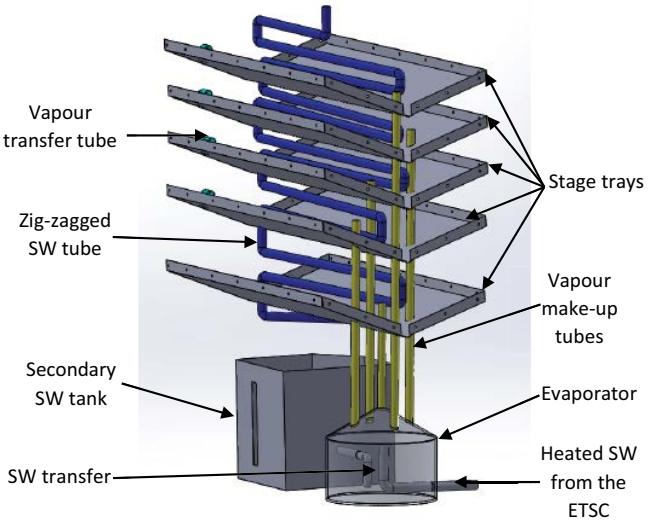

Fig. 3. Vapour-based MSS-SS stages and the evaporator.

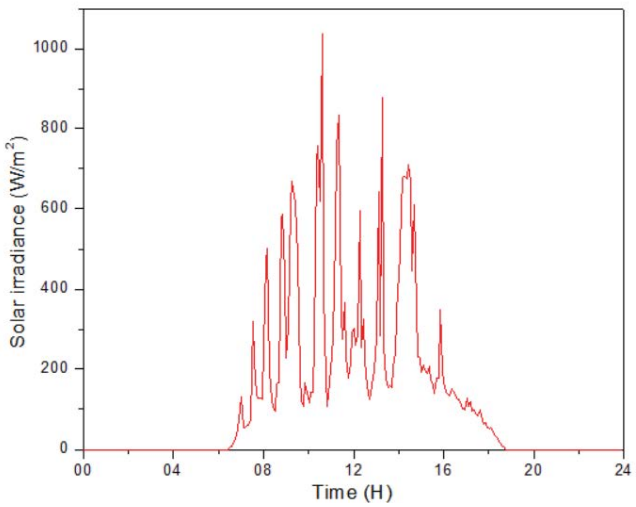

Fig. 4. Solar irradiance vs. time.

from the first recorded to the last recorded solar incident on the day. This curve, through the ETSCs, generated thermal energy to start the desalination process in the condensing tower. The SW temperature profiles in all the stages were the function of this curve.

Furthermore, the wind velocity and ambient temperature graphs shown in Fig. 5 accompanied solar irradiance on the day. The maximum and average wind velocity values were 5.4 and 1.2 m/s, respectively. Wind velocity was more prevalent between 8 AM and 8 PM. Further, the corresponding values for the ambient air temperatures values were 15.4°C and 11.8°C, respectively. The averages were calculated from the day's first and last recorded solar incidence. The ambient air temperature steadily increased with fluctuations and became maximum at around 3 PM. These parameters were necessary since the condensing tower had minimal SW in the stages for cooling down the vapour. Moreover, the polystyrene insulation was completely removed from the body of the condensing tower to observe its behaviour. Under these operating conditions, the surrounding atmospheric conditions influence the temperatures inside the condensing tower [22].

Fig. 6 shows the SW temperature curve of the evaporator, stage wall and stage tray temperatures. Despite the solar irradiance recorded just after 6 AM, Fig. 6 shows a delay in the evaporator SW temperature, which increased sharply around 10 AM. This may be attributed to a low rate of collection by the ETSC in the morning [17]. However, the stage wall and stage tray temperature curves started to increase gradually in the early morning while that of the evaporator was still decreasing in Fig. 6. Again, this may be attributed to the small quantities of vapour entering the stages undetected by the data logger probes. The evaporator curve also shows some fluctuations as it increases, which can be traced back to the solar irradiance curve in Fig. 4.

Moreover, a further delay can be observed between the evaporator curve, stage wall and stage tray in Fig. 6. This delay can be interpreted as due to the thermal boundary the vapour from the evaporator was required to overcome to reach the stages [17,23]. This was due to the cold system components (vapour make-up tubes) in the morning, which created an obstacle for the vapour to flow with less thermal resistance.

Somewhere between 3 PM and 4 PM, the solar irradiance in Fig. 4 shows a sustained increasing curve. For that brief period, thermal energy input assumed a continuous mode, hence the decreased temperature difference in Fig. 6 between the evaporating and condensing surfaces [13]. Therefore, Fig. 6 indicates that when the rate of thermal energy is increased and a continuous mode of thermal energy input assumed, the system is bound to either approach or reach thermal damage condition [13]. Studying the relationship between the stage wall and stage tray in Fig. 6, the stage tray curve was slightly higher than that of the wall from morning until around 3 PM. Around the same time as the solar irradiance curve assumed a continuous mode of thermal energy input, wind velocity at its highest, the stage wall reached 77.6°C. The stage tray and the evaporator SW reached 72.8°C and 90.7°C, respectively.

Fig. 7 presents the SW's temperature curves flowing in the zig-zagged tube in each stage of the condensing tower. Stages 1 to 4 curves in Fig. 7 closely resemble those in Fig. 6, indicating a similar pattern of vapour delivery in those stages. Unlike the MSS-SS with waterbed in the stages where the lower stages maintained higher SW temperatures, thus, higher productivities. The experimental tests on the vapour-based MSS-SS showed a dynamic pattern in terms of which stages maintain higher SW temperatures. In the same period (3 PM to 4 PM) stage 2, stage 1, stage 3, and stage 4 were 78.4°C, 73.6°C, 72.3°C and 53.2°C, respectively. This was because the thermal energy between the stages was not transferred sequentially, among other factors. It can also be noticed that stage 5 curve seems to follow a different path. Two explanations for this are (1) since the initial SW preheating occurred in the BSS, there was an earlier increase in the stage 5 curve in the morning. This may be due to direct preheating by solar radiation in the BSS, and the SW flowed into stage 5. (2) Stage five position relative to the evaporator allowed it to be cooled down sufficiently and maintain low temperatures. The maximum SW temperature in stage 5

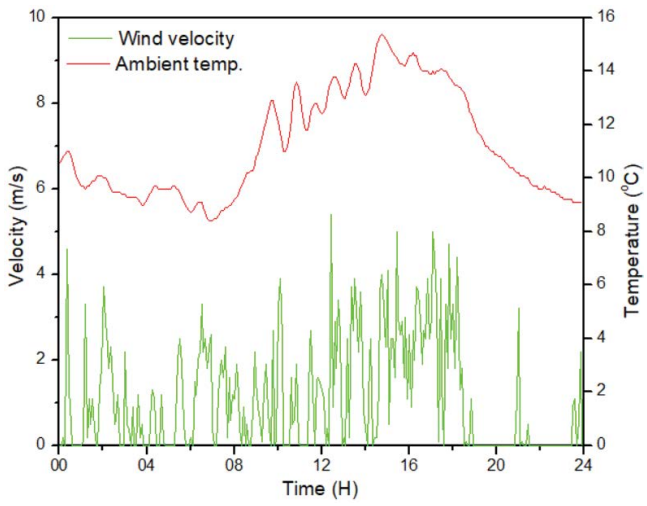

Fig. 5. Wind velocity and ambient air temperature vs. time.

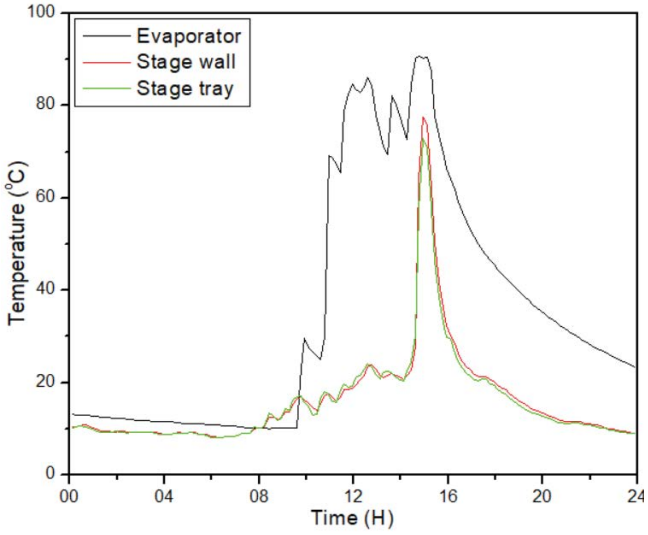

Fig. 6. Evaporative surfaces vs. condensing surfaces.

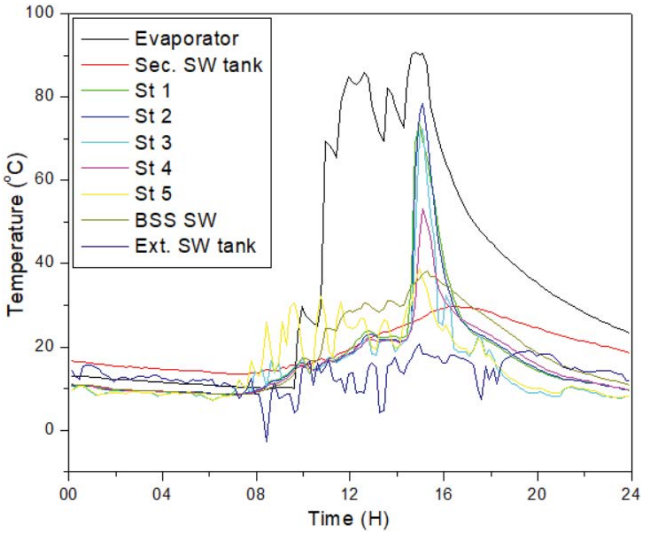

Fig. 7. SW temperature vs. time.

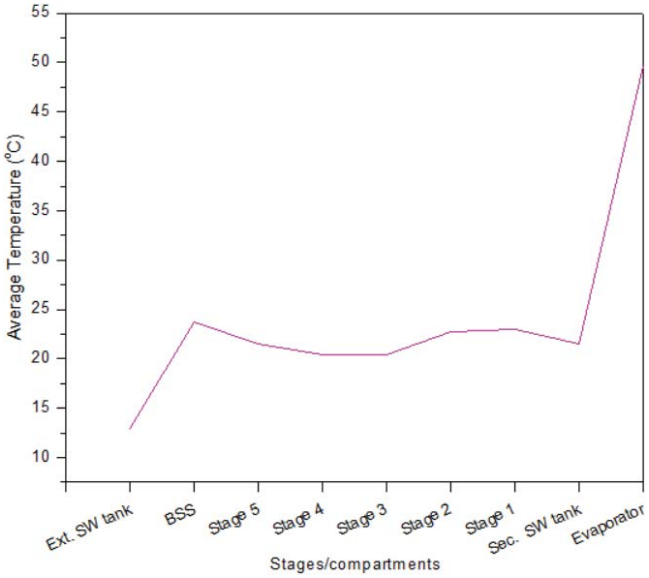

Fig. 8. SW temperature vs. time.

was 38.9°C which occurred around the same period between 3 PM–4 PM.

Meanwhile, the maximum SW temperature in the BSS was 38.2°C. This showed that the SW in stage 5 was preheated by the BSS and the vapour from the evaporator. Theoretically, the vapour entering stage 5 contributed 0.7°C since stage 5, and the BSS SW temperatures were maximum at 38.9°C and 38.2°C, respectively. Furthermore, the secondary tank temperature curve in Fig. 7 shows the cumulative SW temperature increase throughout the system. That is, the initial SW preheating in the BSS and the heat recovery processes in each stage as the SW flowed down through the stages (from stage 5 to stage 1). The external tank temperature was maximum at 20.9°C. At the same time, the secondary tank was at 29.7°C, with a temperature difference of 9.1°C, showing the extent to which SW was preheated before entering the evaporator.

Moreover, Figs. 6 and 7 show a sharp decline in the evaporator SW temperature curve later in the day just before 4 PM. This correlates with the sharp decline in the solar irradiance in Fig. 4, indicating a sharp decrease or a complete halt in the desalination process. Therefore, this points to the system's sensitivity to the varying solar radiation. The direct link between the fashion in which the evaporator SW curve increased relative to the solar irradiance curve was significant. This can be attributed to the SW's low thermal energy storage capacity due to its quantity [18].

Fig. 8 shows the averaged SW temperature in the MSS-SS from the first to the last recorded solar irradiance in Fig. 4. The evaporator SW maintained the highest average temperature as a heat source for the system. The BSS was the second highest implying that the direct heating by solar radiation was effective. In the rest of the stages, the average temperature was according to the extent the SW was preheated. Based on Fig. 8, the contribution from the evaporator through the indirect heating by the ETSCs in terms of preheating the SW in the stages was low compared to that of the direct BSS. This was substantiated by the higher average SW temperature in the BSS.

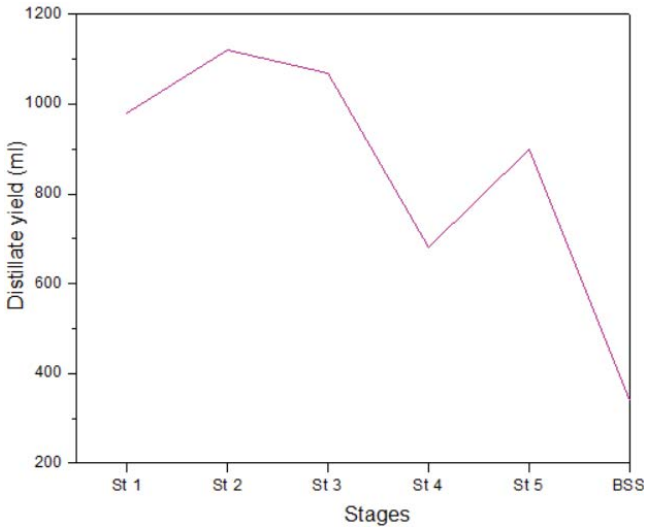

Fig. 9. Distillate yield vs. stage number.

However, the total cumulative SW preheating was represented by the temperature difference between the external tank to the secondary tank 8.6°C. This then suggested that the SW reaching the evaporator was at preheated state. Therefore, the preheating process reduced the amount of energy required to heat and evaporate the SW in the evaporator [24].

Fig. 9 shows the daily distillate yield from each stage of the system. At this point in the development of the vapour-based MSS-SS, the factors influencing the stages' productivity have not been established. An optimisation study would give some insight into these factors. The total cumulative distillate yield achieved was 4,750 mL, excluding that of the BSS, which was 340 mL. The distillate yield trend from stages 1 to 5 was 980; 1,120; 1070; 680 and 900 mL, respectively. Therefore, the total yield from the whole MSS-SS integrated with the BSS was 5,090 mL.

Moreover, from Figs. 6 and 7, stage 2 reached the highest temperature. This means that stage 2 was receiving most vapour from the evaporator. This is contrary to stages 4 and 5 from Figs. 8 and 9; stage 4 reached temperatures higher than stage 5 but produced less distillate than stage 5. This was precisely what was meant when it was stated that factors influencing the stages' productivity were not yet well established.

4.2. Experimental test 2

This subsection discusses the same aspects discussed in subsection 4.1 for the day of 29th of Sept. 2020 with an increased rate of thermal energy input. The prevailing solar irradiance recorded for 10 min longer than on the 26th of Sept. 2020 is shown on Fig. 10. Furthermore, the area under the curve in Fig. 10 is much larger compared to Fig. 4. Therefore, this indicated a higher rate of thermal energy input, assuming a continuous mode rather than impulsive mode [25]. However, its peak was only 817.7 W/m^2, but its average was at 385.7 W/m^2. Moreover, as stated in subsection 4.1, the solar irradiance curve was driving the evaporator curve, which in turn drove the stage curve in conjunction with the BSS curve.

The prevailing wind velocity and ambient air temperature graphs are shown in Fig. 11. The maximum and average wind velocity values were 8.8 and 3.2 m/s, respectively. This indicated an increased wind cooling effect on the condensing tower. Further, the corresponding values for the ambient air temperature values were 17.8°C and 15.5°C, respectively. Given the systems' sensitivity, the ambient temperature values represented a more conducive meteorological conditions for desalination.

Based on the above parameters, Fig. 12 shows the delay between the solar irradiance curve and the evaporator SW as the solar irradiance was available from just after 6 AM (Fig. 10). The evaporator SW temperature only increased sharply around 9 AM. The exact relationship between the stage wall, stage tray, the evaporator SW and the solar irradiance can be observed in Figs. 4, 6 and 7 in the morning. The stage wall and stage tray curves increased while that of the evaporator declined. However, due to the continuous mode of thermal energy input, the evaporator curve increased sharply and maintained temperature around 90°C throughout the day. Moreover, there were fewer fluctuations in the evaporator curve, which correlates with the solar irradiance curve in Fig. 10. The delay between the evaporator curve, stage wall and stage tray curve has decreased.

Furthermore, the stage wall and stage tray curves sharply increased with the evaporator curve indicating an increased rate of thermal energy input. The thermal boundary was quickly overcome, and the vapour delivered in the stages. This suggests that the evaporator contribution to the SW preheating in the stages increased compared to Fig. 7. However, this increased thermal energy input contributed to the reduction in temperature difference between the evaporative and condensing surfaces, threatening thermal damage condition. This was despite the insulation material's

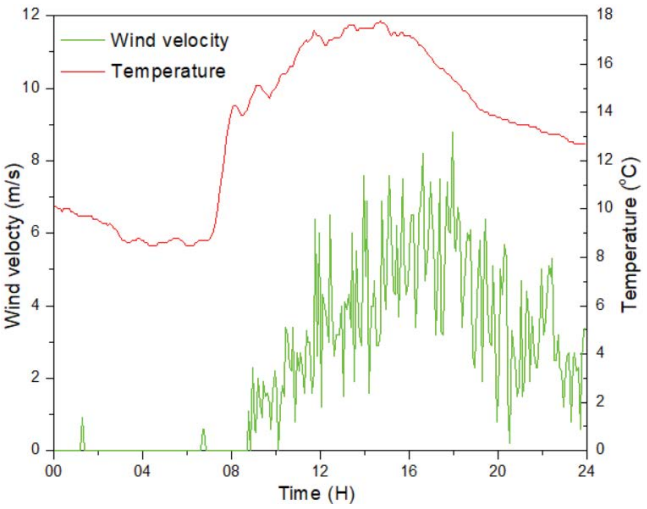

Fig. 11. Wind velocity and ambient air temperature vs. time.

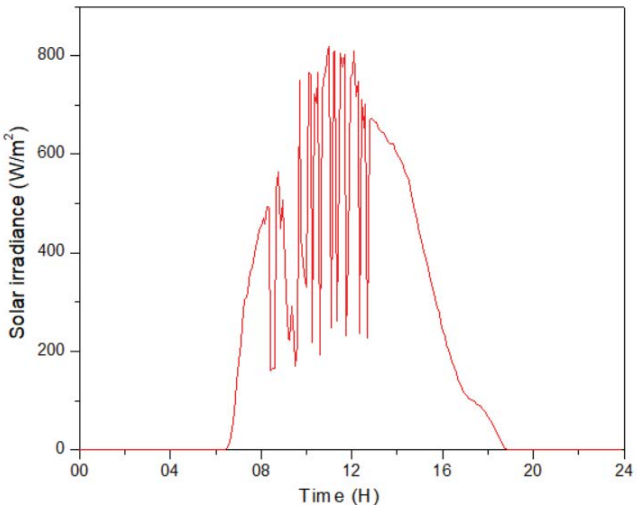

Fig. 10. Solar irradiance vs. time.

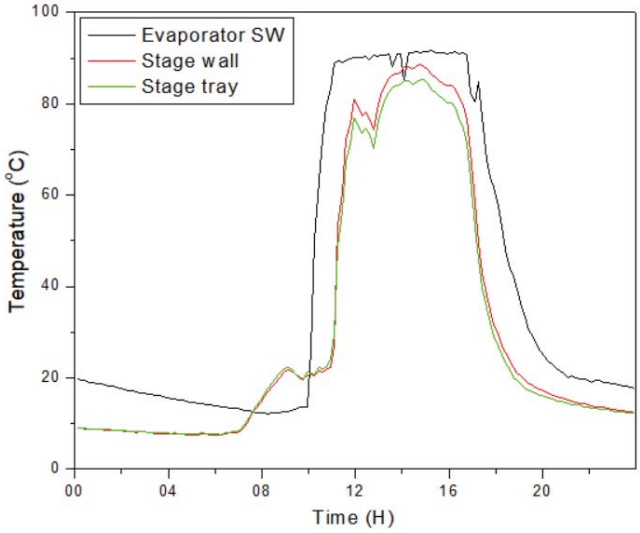

Fig. 12. Evaporative and condensing surfaces vs. time.

absence on the condensing tower's body. The stage wall and stage tray curves analysis show the same trend observed in Fig. 6. The stage wall curve exceeded that of the stage tray in the late morning despite being exposed to the passing winds at average speeds of 3.2 m/s. Fig. 12 suggests that a condensing tower cooling mechanism, without the removal of the thermal insulation, is required to prevent thermal damage conditions. The stage wall and stage tray reached maximum temperature of 88.6°C and 85.4°C, respectively.

The SW temperature curves in Fig. 13 resembles those of Fig. 12; the stage 5 temperature curve increased to 40.4°C, while those of the BSS and the evaporator remained relatively low in the early morning. Stages 1 to 4 also rose slightly, just above the BSS. Therefore, these temperature curve behaviours suggest that SW preheating was contributed by both the evaporator and the BSS. The only question is, to what extent did either the evaporator or the BSS contribute? It was stated under subsection 4.1 that even though the evaporator curve was declining, small quantities undetected by the temperature probes may be entering the stages.

Furthermore, stage 2 maintained the highest temperature despite stage 1 being the closest stage to the evaporator. It is not immediately clear what caused this temperature trend in the vapour-based MSS-SS. Moreover, the stage 4 curve experienced occasional and sudden temperature increases throughout the day; this may be due to the malfunctioning probe or the actual temperature reading of the outer surface of the copper tube where the probe was installed.

The maximum temperatures in stages 1 to 5 were 81°C, 89.5°C, 88.1°C, 120.2°C, and 46.2°C, respectively. These maximum values were higher than those in Fig. 7, putting the condensing tower close to thermal damage condition. Furthermore, as mentioned under subsection 4.1, it can be observed that under this specific rate and mode of thermal energy input, stage 2 was the highest with stage 4 experiencing occasional increases in temperature exceeding that of the evaporator. Moreover, the BSS SW temperature was maximum at 76.1°C suggesting increased heating by solar radiation. Since stage 5 and the BSS were separated by a thin (0.9 mm) sheet of metal, two conclusions can be drawn (1) the vapour condensing on the underside of the sheet metal transferred it latent heat of condensation to the BSS SW and (2) At increased rate of thermal energy input, the BSS SW contributed and maintain stage 5 temperatures relatively lower than other stages since it contained a pool of SW.

Furthermore, the cumulative thermal energy collected throughout the system was reflected in the secondary SW tank, which had a maximum SW temperature of 37.6°C. This maximum secondary SW tank temperature was 7.9°C higher than 29.7°C from the 26th of Sept. 2020. Moreover, the maximum temperature in the external tank was 25.4°C, meaning the temperature difference between the secondary tank and the external tank was 12.2°C. This indicated an increase in SW preheating and heat recovery but represented a threat of thermal damage condition. It can be observed from Figs. 12 and 13 that the evaporator SW temperature curve relative to Fig. 10 declined rapidly later in the day as the solar radiation faded. This indicated a reduction or a complete halt of the desalination process in the condensing tower.

In Fig. 14, the SW temperatures were averaged as indicated in subsection 4.1. Once again, as a thermal energy supplier in the condensing tower, the evaporator SW maintained higher average temperatures. However, unlike in Fig. 8, the evaporator contribution in preheating was evidently more elevated than that of the BSS.

This is shown by stages 1–4, which maintained higher average temperatures than the BSS since the BSS cannot preheat the SW above its own maximum temperatures. Therefore, the change in the mode of thermal energy input also changed the stage's temperature trends compared to those in Fig. 8.

Moreover, the cumulative SW preheating in the system resulted in the average temperature difference of 11.7°C in the external SW tank at 16°C and the secondary SW tank at 27.7°C. This suggested that the SW reaching the evaporator was at preheated state, as in Fig. 8. Also, there has

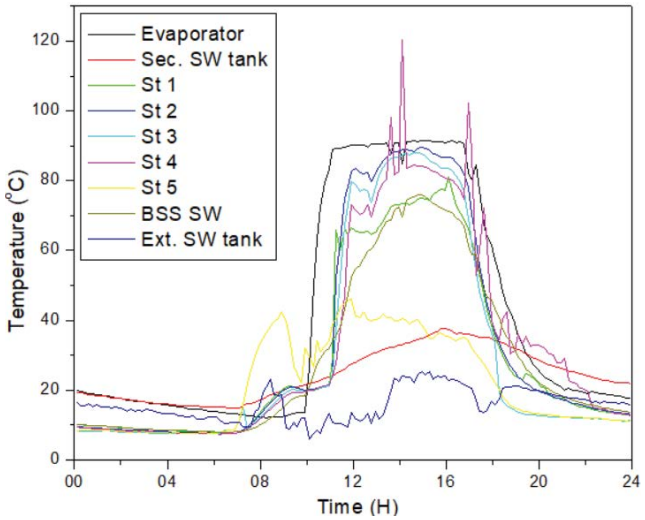

Fig. 13. SW temperature vs. time.

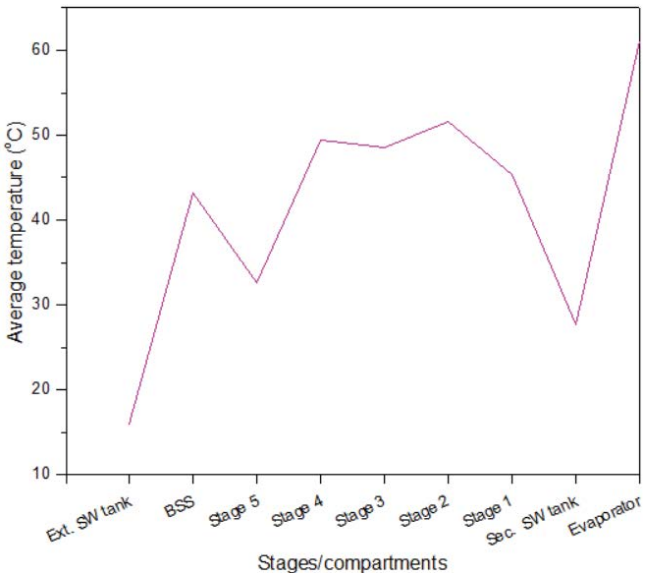

Fig. 14. Average SW temperatures vs. stages/compartments.

Table 1
Summarised data for solar radiation, temperature, and distillate yield variations

Av. solar radiation (W/m^2)			26 Sept. 2020	29 Sept. 2020		Percentage change (%)
			253.7	385.7		52.03 (up)
	Average temperature variation			Distillate yield variation		
	26 Sept. 2020	29 Sept. 2020	Percentage change	26 Sept. 2020	29 Sept. 2020	Percentage change
	Av. SW Temp. (°C)		(%)	Distillate yield (mL)		(%)
Stage 1	24.79	45.37	83.02 (up)	980	1,020	4.08 (up)
Stage 2	24.38	51.61	111.69 (up)	1,120	1,040	7.14 (down)
Stage 3	21.49	48.52	125.78 (up)	1,070	1,050	1.9 (down)
Stage 4	21.93	49.41	125.30 (up)	680	590	13.24 (down)
Stage 5	22.6	32.56	44.07 (up)	900	1,280	42.22 (up)
BSS	25.64	43.23	68.60 (up)	340	480	41.2 (up)
Sec. SW tank	29.7	27.67	6.84 (down)	–	–	–
Ext. SW tank	13.41	16.03	19.54 (up)	–	–	–
Evaporator	54.64	61.14	11.9 (up)	–	–	–

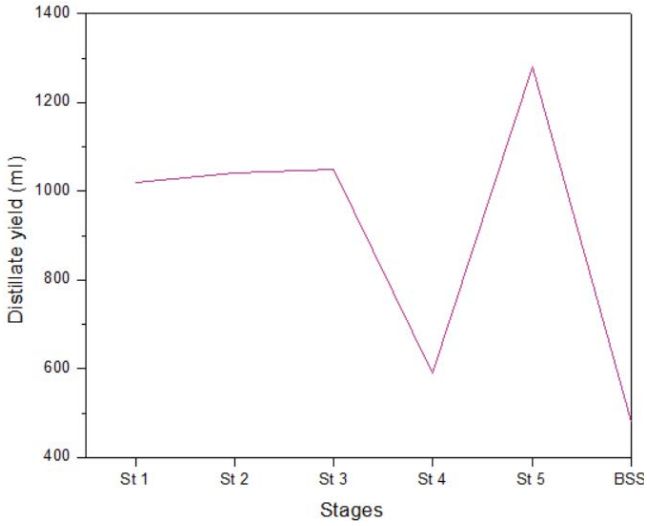

Fig. 15. Distillate yield vs. stage number.

been an increase of 3.1°C between 11.7°C and 8.6°C on the 29th of Sept. 2020 and the 26th of Sept. 2020, respectively. Therefore, an increase in the rate and mode of thermal energy input contributed to the preheating of SW, reducing the amount of energy required to heat and evaporate SW in the evaporator [24].

The distillate yield from each individual stage is shown in Fig. 15. It is immediately apparent that the distillate yield trend of individual stages had changed compared to Fig. 9. In Fig. 15, the trend was 1,020; 1,040; 1,050; 590 and 1,280 mL for stages 1–5, respectively, while it was 480 mL for the BSS. The initial perception was that the higher the stage temperature, the higher its productivity, like in the MSS-SS s discovered in the literature. However, through the experimental observations, the vapour-based MSS-SS showed that stages that maintained relatively low SW temperatures were the most productive. This can be seen for stage 5 in Fig. 15 and can be attributed to the more considerable temperature difference between the evaporative and condensing surfaces. As the temperature difference decreases between the evaporative and condensing surfaces, the desalination process was reduced or even halted since the heat could no longer be transferred between the two surfaces. Stage 4 distillate yield and its temperature was the prime example of a condensing surface that has exceeded the temperature of the evaporative surface. This also suggested that the vapour-based MSS-SS had a larger collector-to-basin area ratio (CBA) [25]. Feilizadeh et al. [25] recommended the augmentation of thermal energy storage (TES) devices where the CBA is larger.

Furthermore, when the thermal damage condition occurs, there is pressure build-up which causes the vapour to leak to the atmosphere or transfer to another stage. The means to transfer the vapour in case of pressure build-up was built into the system (Figs. 1 and 3). However, the minimal SW in the stages could not sufficiently cool down the vapour in the stages. Moreover, the wind velocities were also unable to assist in maintaining a larger temperature difference.

Table 1 shows the summarised results from the two experimental days. A 52.03% increase in average solar radiation resulted in the SW temperature change in each compartment of the tower. As it can be observed for stages 2, 3, and 5 that the distillate yield was negatively affected due to thermal dagame conditions which impeded the desalination process. However, stages 1, 5 and the BSS experienced increased distillate outputs as stage temperatures remained relatively low. The 42.22% and 41.2% increase in stage 5 and the BSS distillate yields were direct results of the larger body of SW in the BSS with increased cooling effects.

Furthermore, despite an 11.9% increase in the evaporator temperature indicating enhanced evaporation, the average cumulative heat recovery and SW preheating were reduced by 6.84% in the secondary SW tank. With the absence of insulation on the body of the condensing tower, the cumulative heat recovery and SW preheating processes were ineffective as rapid heat losses were encountered. There was a distinct behavior driven by the mode of thermal energy

input between the 2 d. Under continuous mode, the condensing tower required TES as increasing the average solar radiation by 52.03% contributed to increased heat losses and very little improvement in distillate yield.

5. Conclusion

The experimental results obtained from tests conducted on a novel vapour-based MSS-SS were presented in this work. The study found that the stage SW temperatures were dynamic and linked to the modes of thermal energy input. Stage temperature behaviours were also inversely related to the distillate yield trends owing to the temperature difference in a stage. Due to the larger CBA, the impulsive mode of thermal energy input maintained a larger temperature difference between the evaporative and condensing surfaces suitable for sustaining the desalination process. However, the continuous mode caused thermal damage condition due to the critical reduction in temperature difference. The larger CBA also contributed to the enhanced evaporation as SW maintained temperatures of approximately 90°C during sunshine hours. Furthermore, the rapid decline in SW temperature later in the day indicated SW's inadequate thermal storage capacity and the absence of insulation material. Increasing the average solar radiation by 52.03% enhanced the cumulative distillate yield by 3.97% and 7.27% for stages 1 to 5 and the entire condensing tower, respectively.

Future work

- The quantity of SW flowing in the stages should be increased to help with its thermal energy storage capacity.
- A TES device be incorporated into vapour-based MSS-SS to prevent thermal damage conditions.
- A single ETSC will be sufficient to power the vapour-based MSS-SS.
- A detailed study to establish the distillate yield trend of the stages is necessary.
- The reduced overall height of the system may contribute to reducing the thermal boundary in the vapour make-up tubes and more vapour reaching the stages
- An optimization study of the vapour-based MSS-SS will assist in understanding the system better,

Declaration of interest

The authors have no declaration of interest.

Acknowledgements

Authors would like to thank the National Research Foundation for financial support.

References

[1] E. Sartori, Solar still versus solar evaporator: a comparative study between their thermal behaviors, Sol. Energy, 56 (1996) 199–206.
[2] S. Kumar, A. Dubey, G.N. Tiwari, A solar still augmented with an evacuated tube collector in forced mode, Desalination, 347 (2014) 15–24.
[3] K.S. Reddy, K.R. Kumar, T.S. O'Donovan, T.K. Mallick, Performance analysis of an evacuated multi-stage solar water desalination system, Desalination, 288 (2012) 80–92.
[4] A.F. Muftah, M.A. Alghoul, A. Fudholi, M.M. Abdul-Majeed, K. Sopian, Factors affecting basin type solar still productivity: a detailed review, Renewable Sustainable Energy Rev., 32 (2014) 430–447.
[5] R.K. Lal, S. Mishra, J.P. Dwivedi, H. Dwivedi, A comprehensive study of the different parameters of solar still, Mater. Today:. Proc., 4 (2017) 3572–3580.
[6] D. Mowla, G. Karimi, Mathematical modelling of solar stills in Iran, Sol. Energy, 55 (1995) 389–393.
[7] V. Sivakumar, E.G. Sundaram, Improvement techniques of solar still efficiency: a review, Renewable Sustainable Energy Rev., 28 (2013) 246–264.
[8] A.A. El-Sebaii, On effect of wind speed on passive solar still performance based on inner/outer surface temperatures of the glass cover, Energy, 36 (2011) 4943–4949.
[9] R.S. Adhikari, A. Kumar, G.D. Sootha, Simulation studies on a multi-stage stacked tray solar still, Sol. Energy, 54 (1995) 317–325.
[10] K. Schwarzer, M.E. Vieira, C. Faber, C. Müller, Solar thermal desalination system with heat recovery, Desalination, 137 (2001) 23–29.
[11] B.A. Jubran, M.I. Ahmed, A.F. Ismail, Y.A. Abakar, Numerical modelling of a multi-stage solar still, Energy Convers. Manage., 41 (2000) 1107–1121.
[12] K. Schwarzer, E.V. da Silva, B. Hoffschmidt, T. Schwarzer, A new solar desalination system with heat recovery for decentralised drinking water production, Desalination, 248 (2009) 204–211.
[13] M.I. Shatat, K. Mahkamov, Determination of rational design parameters of a multi-stage solar water desalination still using transient mathematical modelling, Renewable Energy, 35 (2010) 52–61.
[14] J. Franco, L. Saravia, A new design for a passive atmospheric multistage still, Renewable Energy, 4 (1994) 119–122.
[15] A. Abdessemed, C. Bougriou, D. Guerraiche, R. Abachi, Effects of tray shape of a multi-stage solar still coupled to a parabolic concentrating solar collector in Algeria, Renewable Energy, 132 (2019) 1134–1140.
[16] Z. Chen, J. Peng, G. Chen, L. Hou, T. Yu, Y. Yao, H. Zheng, Analysis of heat and mass transferring mechanism of multi-stage stacked-tray solar seawater desalination still and experimental research on its performance, Sol. Energy, 142 (2017) 278–287.
[17] M.K. Estahbanati, M. Feilizadeh, K. Jafarpur, M. Feilizadeh, M.R. Rahimpour, Experimental investigation of a multi-effect active solar still: the effect of the number of stages, Appl. Energy, 137 (2015) 46–55.
[18] A. Soni, J.A. Stagner, D.S.K. Ting, Adaptable wind/solar powered hybrid system for household wastewater treatment, Sustainable Energy Technol. Assess., 24 (2017) 8–18.
[19] P. Singh, P. Singh, J. Singh, R.I. Singh, K. Kundu, Performance Evaluation of Low Inertia Multi-Stage Solar Still, Proceedings of the International MultiConference of Engineers & Computer Scientists 2012, Vol. II, 2012, pp. 1–6. 2012.
[20] O. Bait, M. Si-Ameur, Numerical investigation of a multi-stage solar still under Batna climatic conditions: effect of radiation term on mass and heat energy balances, Energy, 98 (2016) 308–323.
[21] M.M. Mkhize, V. Msomi, A comparative study of the multistage solar stills with stacked stages (MSS-SS), J. Eng., 2021 (2021) 7751442, doi: 10.1155/2021/7751442.
[22] S. Kumar, V.K. Dwivedi, Experimental study on modified single slope single basin active solar still, Desalination, 367 (2015) 69–75.
[23] Y.A. Çengel, R.H. Turner, J.M. Cimbala, M. Kanoglu, Fundamentals of Thermal-Fluid Sciences, McGraw-Hill, New York, 2008.
[24] F. Saeedi, F. Sarhaddi, A. Behzadmehr, Optimization of a PV/T (photovoltaic/thermal) active solar still, Energy, 87 (2015) 142–152.
[25] M. Feilizadeh, M.K. Estahbanati, A.S. Ardekani, M.E. Zakeri, K. Jafarpur, Effects of amount and mode of input energy on the performance of a multi-stage solar still: an experimental study, Desalination, 375 (2015) 108–115.